sustainability

MDPI

Article

Biogenic Synthesis of Silver-Iron Oxide Nanoparticles Using Kulekhara Leaves Extract for Removing Crystal Violet and Malachite Green Dyes from Water

Haradhan Kolya * and Chun-Won Kang *

Department of Housing Environmental Design, Research Institute of Human Ecology, College of Human Ecology, Jeonbuk National University, Jeonju 54896, Republic of Korea

* Correspondence: haradhankoley@gmail.com or hdk@jbnu.ac.kr (H.K.); kcwon@jbnu.ac.kr (C.-W.K.)

Abstract: Crystal violet and malachite green, cationic dyes, are widely used in various industries. Water-containing dye molecules affect human health and aquatic life. Here, we synthesized silver-iron oxide nanoparticles using an aqueous extract of kulekhara leaves. The main advantage of this synthesis is that no iron salts were used to prepare Ag-iron oxide nanoparticles. Iron-rich Kulekhara leaves provide iron oxide during the in situ formation of silver nanoparticles. Synthesized Ag-Fe_2O_3 nanoparticles were characterized by UV-Vis, FTIR, XRD, and STEM-Cs. The dye-degradation studies were performed using synthesized nanoparticles in the presence of sodium borohydride. In the catalytic reaction, the color of crystal violet and malachite green disappeared (100%) within three minutes, and the same results were obtained in their mixtures (1:1 v/v). The presence of Fe_2O_3 in AgNPs may boost the rapid reduction in azo bonds due to the higher exposed surface area. The color changes were monitored using UV-Vis spectroscopy. Comparative literature studies showed that the performance of Ag-Fe_2O_3 is superior regarding the degradation of malachite green and crystal violet. These findings could entice researchers to design and develop various dye degradation using this eco-friendly process.

Keywords: green synthesis; silver nanoparticles; malachite green; crystal violet; catalytic degradation; mixture dyes

Citation: Kolya, H.; Kang, C.-W. Biogenic Synthesis of Silver-Iron Oxide Nanoparticles Using Kulekhara Leaves Extract for Removing Crystal Violet and Malachite Green Dyes from Water. *Sustainability* **2022**, *14*, 15800. https://doi.org/10.3390/su142315800

Academic Editor: Danilo Spasiano

Received: 6 October 2022
Accepted: 24 November 2022
Published: 28 November 2022

1. Introduction

A constant supply of pure water is required in the home and industrial sectors. Waterways, lakes, and subsurface resources provide most water for domestic and industrial use. Freshwater resources are decreasing and becoming more and more contaminated as the global population and industrialization increase. Industries frequently use clean, sweet water while polluting rivers and seas. Crystal violet (CV) and malachite green (MG) dyes are commonly used in the textile, leather, wood, and paper industries [1,2]. Some dyes are loosely bound with textiles but may seep out of clothes when washed [3]. Therefore, textile industries produce coloring effluents and discharge them into rivers or seawater without proper treatment.

On the other hand, the aqueous dye solutions used to stain microorganisms are often discharged directly into the drain water [4,5]. Dye molecules in water cause several toxicities in marine life and human health [6]. Dyes, in this case, crystal violet and malachite green, which are hydrosoluble, would hinder the penetration of sunlight into the deep, reduce the solubility of oxygen in water, and thus hamper the ecosystem in water bodies [7]. However, most synthetic dyes create various public health diseases such as headaches, hypertension, red blood cell breakdown, skin allergy, central nervous system disorder, and cancer [8]. Therefore, research into removing dyes from water is crucial for ecological sustainability.

Several wastewater treatment technologies are available for removing dyes and other pollutants from wastewater, such as adsorption [9–11], membrane filtration [12],

flocculation [13], advanced oxidation, bacterial degradation [14], and catalytic degradation [15,16]. The inexpensive process cost and less sludge generation/regeneration adsorption [17,18] and catalytic degradation methods [19] entice researchers in these studies. At present, biopolymer-based adsorbents are an attractive research area for wastewater treatment [20]. In addition, nanoparticles and magnetic-nanoparticles or magnetic polymer nanocomposites materials [21–23] are attracting attention among researchers in catalytic degradation [24,25] and adsorption processes [26] due to their easy regeneration, reusability, low cost, and less sludge [27–30].

Catalytic reduction in sodium borohydride has received particular attention for degrading dye molecules [31,32]. Sodium borohydride plays an essential catalytic role as a co-catalyst that can provide electrons and hydrogen in the catalytic dye degradation [33]. Furthermore, variations in color intensity might be easily monitored using UV-Vis spectroscopy. The azo bonds in azo dye molecules could be readily cleaved by hydrogenation, resulting in the dye molecules changing into less hazardous and environmentally friendly products. Researchers used various catalytic systems for azo bond cleavage, especially metal/metal oxide nanoparticles [34,35].

On the other hand, many surfactants and reactants are utilized to form and stabilize metal nanoparticles [36]. These chemicals are hazardous to the environment and humans. Therefore, environmentally friendly processes should produce and use metal nanoparticles. Researchers have recently used various fruit extracts [37], leaf extracts [38], and flower extracts [39] to prepare silver nanoparticles. Silver nanoparticles have unacceptable toxic effects on human health and the environment, in addition to their antimicrobial activity [40].

In this study, we synthesized silver-iron oxide nanoparticles using kulekhara leaves (*Hygrophila auriculata*) extract. This is an eco-friendly, facile, and low-cost approach. Kulekhara leaves are used as traditional medicinal plants in India [41,42]. Kulekhara leaves contain iron (Fe^{+2}) and vitamin C are higher than common greens such as spinach, lettuce, and coriander. The leaves also contain many phytochemicals: flavonoids, glycosides, phenolic components, tannins, etc. [43]. These phytochemicals usually act as reducing and stabilizing agents to form metal nanoparticles [44]. In addition, Fe^{+2} has an essential role in forming naturally occurring silver nanoparticles [45]. As a result, dissolved Fe^{+2}, and Ag^{+} transformed into Fe^{+3} and Ag^{0}, respectively. The presence of phenolic-rich components in the leaf extract results in forming Fe_2O_3 simultaneously [46]. Synthesized materials were characterized by UV-Vis spectroscopy, FTIR spectroscopy, XRD, and STEM-Cs; the findings are discussed below.

2. Materials and Methods

2.1. Materials

Silver nitrate and borohydride were purchased from Sigma Aldrich, Korea. MG and CV dyes were procured from Daejung Chemicals & Metals Co. Ltd., Siheung, Republic of Korea. Distilled water was used for the entire synthesis process, and tap water (pH 6.9, turbidity 0.1 NTU) was used to prepare a stock solution of 100 mg/L, MG, and CV dyes. Kulekhara leaves were obtained from Indian marketplaces.

2.2. Preparation of Nanoparticles

Green kulekhara leaves were collected from Rajabazar market, Midnapore, West Bengal, India. Green leaves were dried under sunlight, and drying leaves were pulverized using a mixer grinder. The dust of leaves (500 mg) was poured into water (100 mL) and then boiled for about 10 min. After filtering the residue, the filtrate was collected in a stoppered conical flask and used to synthesize nanoparticles. About 50 mL (10^{-3} M) of silver nitrate aqueous solution was taken in a beaker, and then 2 mL of kulekhara leaves extract was mixed with the solution at room temperature (24 °C). The solution color changed from colorless to yellowish within 5 min, and then the yellowish color transformed to a deep radish yellow within 10 min. This solution was subjected to characterization using instrumental characterization techniques. A schematic of the synthesis process is shown in Figure 1.

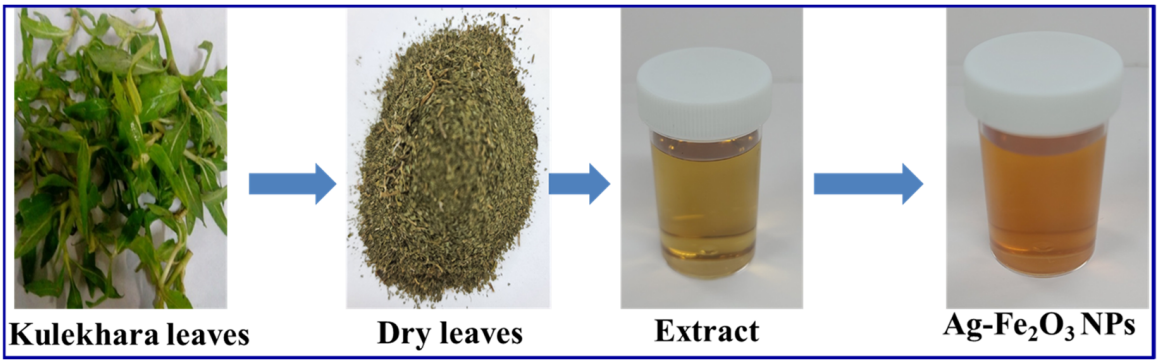

Figure 1. Schematic of silver-iron oxide nanoparticle synthesis.

2.3. Characterization

UV-Vis spectrophotometer (UV−1650PC, Shimadzu, Kyoto, Japan) was utilized to measure the optical characteristics of the colored solution. The absorbance spectra were collected in a 1 cm cuvette at an 800–200 nm wavelength. FTIR spectra (Thermo Scientific Nicolet iS20, Waltham, MA, USA) in the wavelength range 4000–400 cm^{-1} were used to investigate the change in chemical functionality and nanoparticle formation using KBr pellets. The colloidal solution was centrifuged, and the residue was dried on glass plates in a vacuum oven at 80 °C. The dried materials were structurally examined using an X-ray diffractometer (Miniflex, Rigaku, Japan), Cu Kα radiation at a scan rate of 1° min^{-1} in the 10–80° range. The drop-casting technique was used to obtain sufficient material for TEM analysis on a lacey F/C 300 mesh Cu grid. High-resolution transmittance electron spectroscopy (STEM-Cs, JEOL/JEM-ARM200F) at 200 kV was used for morphological investigation and EDS analysis.

2.4. Removal of Malachite Green and Crystal Violet

In a 100 mL conical flask, 35 mL of MG (100 mg/L) and CV (100 mg/L) dyes were taken separately. The dye solution was then mixed with 1 mL of $NaBH_4$ (0.5 mg/mL) by handshaking. After that, 0.5 mL of nanoparticle solution was added to the mixture. The azo bonds of the MG and CV dyes were rapidly destroyed, and the solution became colorless.

On the other hand, 3 mL of MG or CV dyes were taken in UV-cuvette, and then 20 µL of prepared $NaBH_4$ solution was added. After that, 20 µL of nanoparticle solution was added and mixed quickly. Afterward, UV-Vis measurements were performed at an interval of 1 min in the 800–200 nm range (scan speed: fast, sampling interval: 0.5 nm). A mixture of these two dye solutions was prepared by mixing two equal volumes of each dye (1:1 *v*/*v*). The procedure, as mentioned earlier, was used to investigate the degradation of dyes in the mixture.

3. Results and Discussions

3.1. Synthesis and Characterization of Ag-Fe_2O_3 Nanoparticles

The nanoparticle solution had a specific color change compared to the extract solution, as illustrated in Figure 1. Figure 2a shows the UV-Vis spectra of nanoparticles, kulekhara extract, and silver nitrate solution.

The absorbance peak at 429 nm suggests the presence of silver nanoparticles. The formation of silver nanoparticles by Fe^{+2} was found to have significant absorbance between 350 nm and 700 nm, indicating a polydispersed distribution of AgNPs/Fe_2O_3 [45]. The peak at 290 nm suggests the presence of natural phenolic compounds (phytochemicals) in the kulekhara leaf extract [47,48].

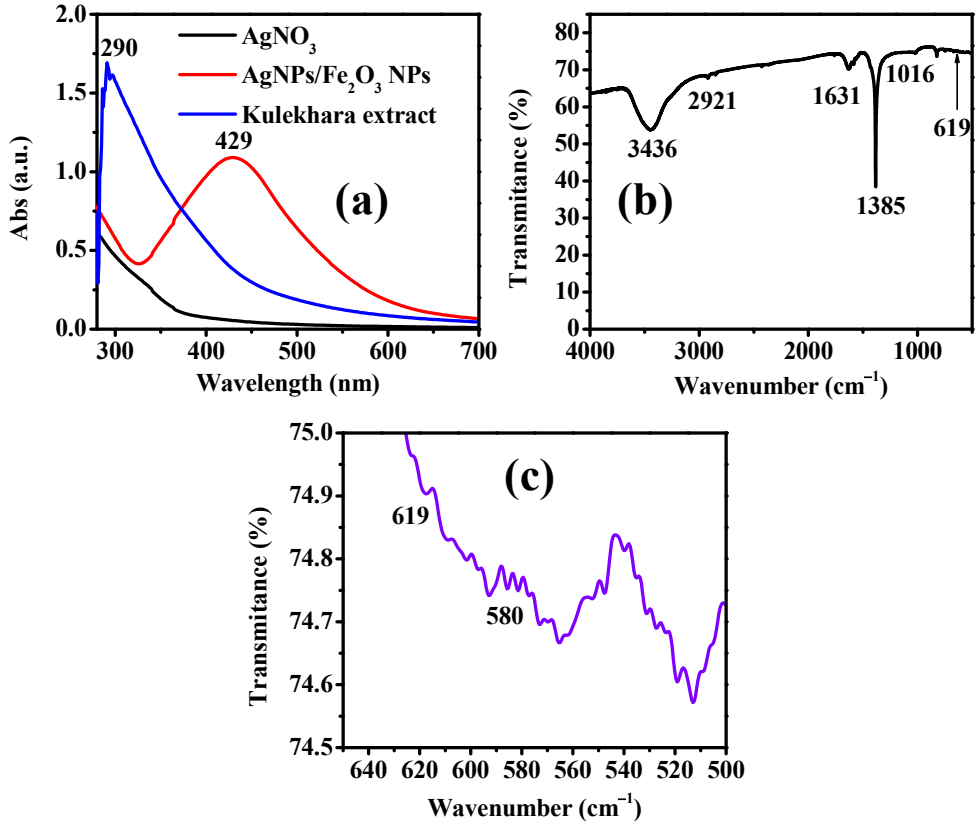

Figure 2. (**a**) UV-Vis spectra of silver/Fe_2O_3 nanoparticles, kulekhara extract, and silver nitrate solution, (**b**) FTIR spectra of Ag/Fe_2O_3 nanoparticles, and (**c**) zoom view of FTIR spectra of Ag/Fe_2O_3 nanoparticles.

The FTIR spectrum of the eco-friendly synthesized Ag/Fe_2O_3 nanoparticles is shown in Figure 2b. The O—H bond stretching in phenolic compounds appeared at 3436 cm^{-1}. The peak at 2921 cm^{-1} and 1631 cm^{-1} corresponds to the —CH stretching of the methylene group and C=C stretching, respectively. The high peak at 1385 cm^{-1} confirms the presence of silver nanoparticles [15]. The peak in the C—O stretching, O—H vibration, or C—O—C bond vibration is 1016 cm^{-1} [47]. Moreover, the Fe—O stretching band's vibration coincides at 580 cm^{-1} and 619 cm^{-1} (Figure 2c) [25,49].

The crystalline nature of the synthesized nanoparticle using the XRD spectrum is shown in Figure 3.

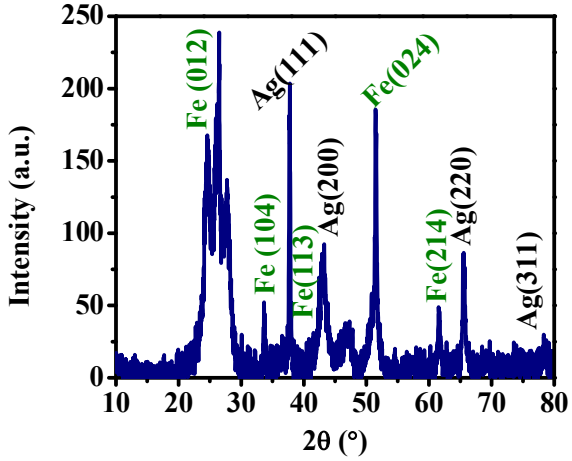

Figure 3. XRD diffraction pattern of Ag/Fe_2O_3 nanoparticles by kulekhara leaves extract.

The presence of amorphous peaks in the spectrum implies the green synthesis of nanoparticles. The peak at 10°–20° refers to organic components from the reaction medium responsible for stabilizing the formed nanoparticles [25]. The peaks at 38°, 43.4°, 65.5°, and 77.1° are formed by the lattice planes of face-centered cubic silver crystals (111), (200), (220), and (311), respectively. The obtained data were matched with the JCPDS database:04–0783 [50]. On the other hand, peaks at 24.5°, 33.6°, 41.0°, 51.5°, and 62.6° corresponds to the X-ray diffraction pattern of Fe_2O_3 and indicate lattice plane (012), (104), (113), (024) and (214) respectively [51]. Therefore, the XRD spectrum indicates the formation of Ag/Fe_2O_3 nanoparticles.

The morphology of the Ag/Fe_2O_3 nanoparticles was also investigated by STEM-Cs analysis. TEM images of nanoparticles are shown in Figure 4a,b at different magnifications. TEM analyses (Figure 4a,b) reveal that relatively spherical nanoparticles are formed with an average diameter of 10.42 ± 0.81 nm. The size distribution histogram is shown in Figure 4c. The HR-TEM image of $AgNPs/Fe_2O_3$ nanoparticles (Figure 4d) demonstrates the lattice fringes. The nearly smooth edges are also quite distinct from this image. Energy dispersive X-ray analysis (EDS) elemental mapping was used to identify the elements present in the prepared nanoparticles. The EDS mapping and layer image of elements O, Fe, and Ag are shown in Figure 4e–h. The EDS mapping demonstrates that oxygen and iron are associated with the particles on silver nanoparticles (Figure 4h). The overall analysis of TEM images indicates the formation of Ag-iron oxide nanoparticles by kulekhara leaves extract.

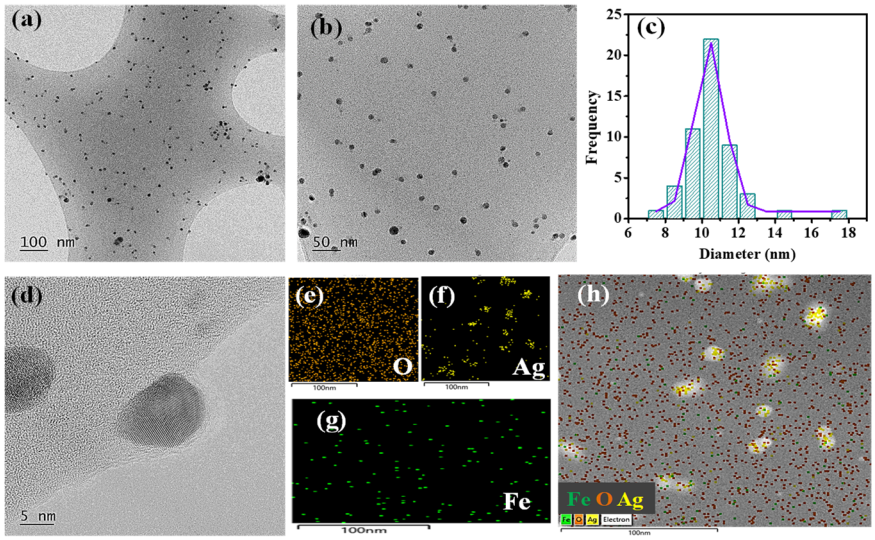

Figure 4. STEM-Cs images at different magnifications (**a**) 100 nm, (**b**) 50 nm, (**c**) histogram of size distribution using ImageJ and originPro 8.5 software, (**d**) HR-TEM single crystal at 5 nm, (**e**) mapping of O, (**f**) mapping of Ag, (**g**) mapping of Fe, and (**h**) EDS layer image of elements.

3.2. Catalytic Activity of Ag-Iron Oxide Nanoparticles

The UV-Vis spectrophotometer was used to determine the catalytic activity of the synthesized nanoparticles for the hydrogenation reaction of azo bonds in crystal violet, malachite green, and their mixtures. The results are shown in Figure 5. Color changes and the UV-Vis spectra before and after the catalytic reaction are shown in Figure 5a. The maximum absorbance (λ_{max}) of crystal violet appeared at 588 nm. After adding nanoparticles, its intensity slightly increases due to the interaction between dye molecules and nanoparticles. A new peak appeared at 420 nm as a result of the presence of Ag and Fe_2O_3 nanoparticles. After adding sodium borohydride, the peak intensity at 588 nm decreases very quickly, and the absorbance becomes almost zero within 3 minutes. A new peak appeared at 286 nm, which is due to the reduction in crystal violet and the formation of leucocrystal violet [52]. The degraded crystal violet, leucocrystal violet, did not show any toxicity in water, as confirmed by the studies of Sengan et al. [31] using the Zebrafish model.

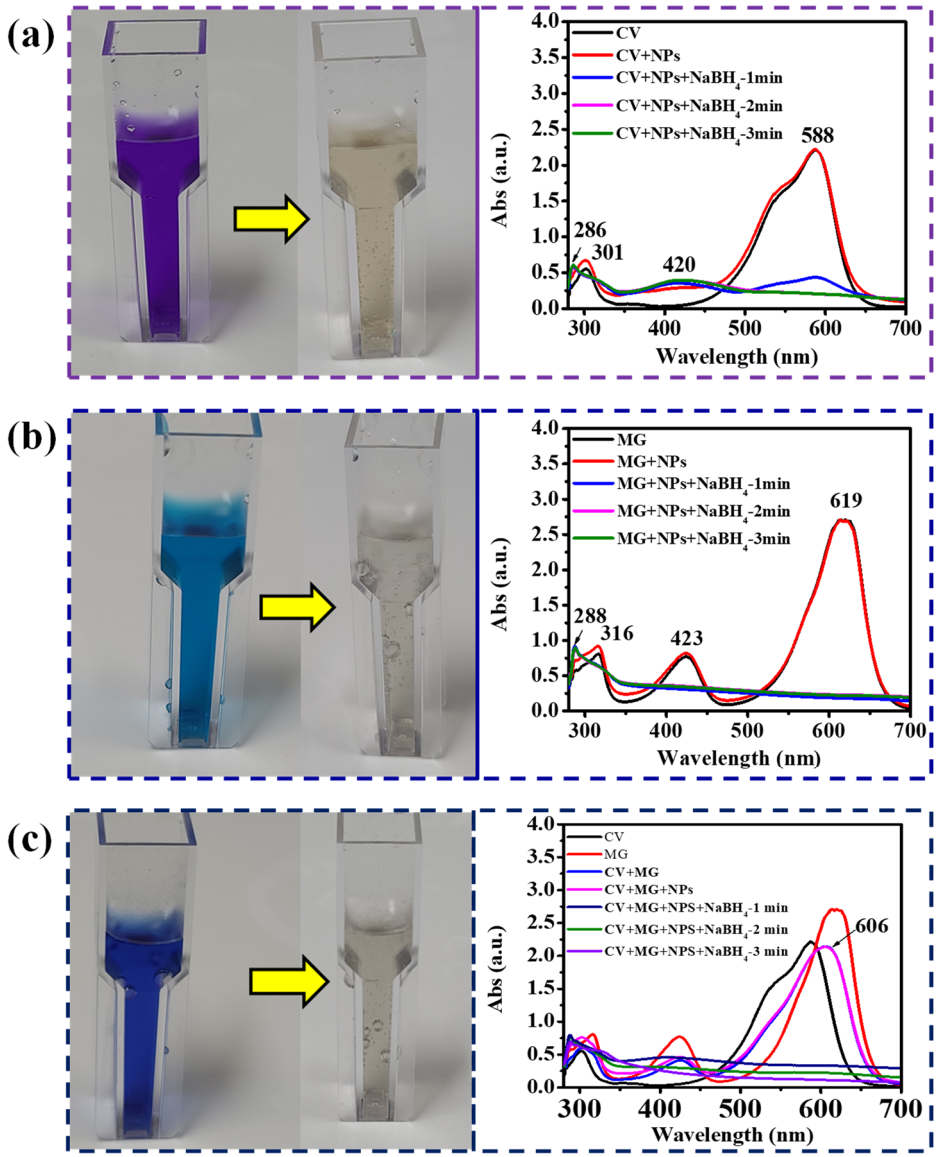

Figure 5. Dye degradation studies (**a**) crystal violet, (**b**) malachite green, and (**c**) mixtures of crystal violet and malachite green.

On the other hand, the maximum absorbance peak in malachite green dye was observed at 619 nm, as shown in Figure 5b. The intensity of the peak pattern decreases, and the absorbance becomes zero after three minutes of adding nanoparticles and sodium borohydride solution. The peak appeared at 288 nm, suggesting the formation of leucomalachite green [53]. Similarly, the reduction in their (CV + MG; 1:1 v/v) mixture by nanoparticles in the presence of sodium borohydride exhibited complete reduction within 3 minutes (Figure 5c). However, a slow reduction reaction of azo bonds was observed using only sodium borohydride.

Additionally, there was no difference in absorption in the absence of sodium borohydride. Moreover, the reduction in azo bonds took place more quickly in the presence of Ag-Fe_2O_3 nanoparticles and $NaBH_4$. This is due to the greater availability of exposed surface area of nanoparticles. The catalyst accepts electrons from BH_4- ions and transfers them to electrophilic dyes, thereby initiating catalytic reduction. The donor is BH_4- and the acceptor is the dye molecule. The dye molecules' electrons are then transferred to the catalyst [54]. A probable mechanism is shown in Figure 6.

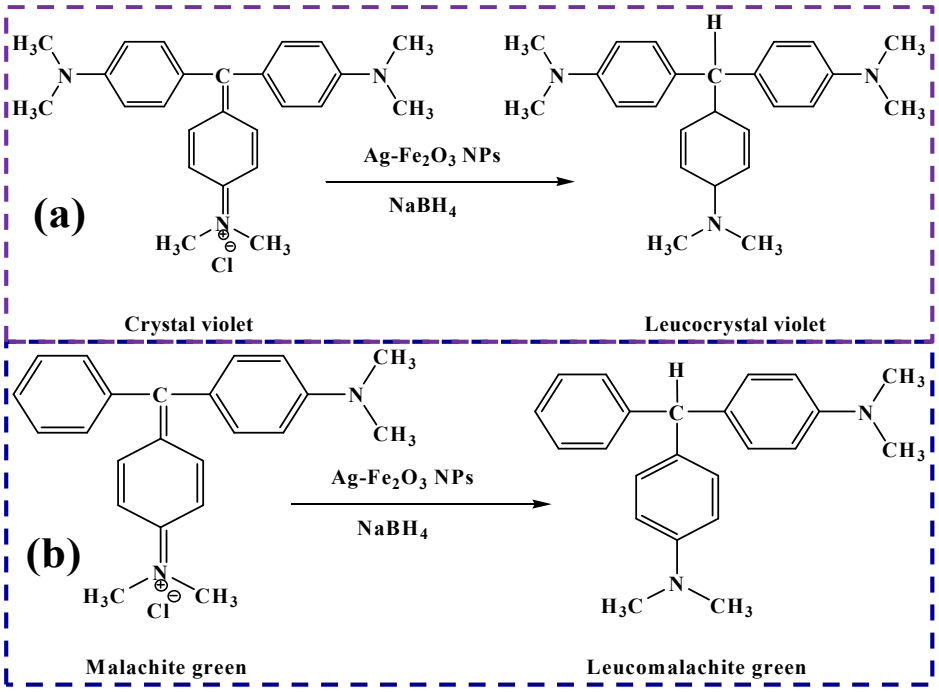

Figure 6. Reaction mechanism of azo bonds reduction using nanoparticles and sodium $NaBH_4$, (**a**) crystal violet and (**b**) malachite green.

3.3. Discussion

A simple and environmentally friendly method was used to prepare silver–iron oxide nanoparticles. This study used kuleakhara leaf extract as a reducing agent and iron supplier in the reaction medium. As kulekhara leaves contain enough ferrous compounds, iron salts from outside are not used. On the other hand, phytochemicals and iron(II) in leaf extracts can reduce the silver ion [41,42]. The presence of phenolic-rich components and iron(II) in the leaf extract resulted in the formation of Fe_2O_3, as iron(II) was oxidized to iron(III), and silver(I) was reduced to silver(0) [46]. The UV-Vis, FTIR, XRD, and TEM characterization techniques confirmed the formation of these nanoparticle. The nanoparticles were used as a catalyst to reduce the azo bond in the dye molecules in the presence of sodium borohydride. We investigated the catalytic performance of Ag/Fe_2O_3 nanoparticles using two cationic dyes (malachite green and crystal violet) separately and in combination. Nanoparticles with $NaBH_4$ cleaved azo bonds quickly, and discoloration was complete in three minutes. The formation of leucocrystal violet and leucomalachite green is recognized by the discoloration of the solutions [52,53]. However, there was no dye discoloration using nanoparticles without $NaBH_4$. The reaction rate of sodium borohydride to reduce the azo bond of dye molecules is slow.

Furthermore, the reduction in azo bonds was accelerated in the presence of $Ag\text{-}Fe_2O_3$ nanoparticles. This is due to the increased availability of nanoparticle exposed surface area. The elemental composition of the treated dye mixture (supernatant liquid) was evaluated by EDS. The percent composition was as follows: C (89.01%), N (5.92%), O (4.92%), Fe (0.05%), and Ag (0.09%). It is difficult to separate the catalyst from the reaction medium and thus to test its reusability due to the low concentration of Ag and Fe in the treated solution. Further research is needed to study the magnetic properties of Ag-iron oxide nanoparticles.

3.4. Efficiency Comparison

The catalytic efficiency of Ag-iron oxide nanoparticles for the degradation of dyes' molecules was compared to other metal nanoparticles and other dyes, as shown in Table 1. Methylene blue is the most reported dye in literature. The reduction in methylene blue with

silver nanoparticles and $NaBH_4$ is faster compared to catalytic reduction with silver nanoparticles only. Bentonite-AgNPs could remove 84.6% of malachite green in 5 min. However, Ag-Fe_2O_3 nanoparticles removed 100% of malachite green and crystal violet in 3 min. It is evident that the green synthesized Ag-iron oxide nanoparticles exhibited better efficiency than some other green synthesized silver nanoparticles using different leaf extracts.

Table 1. Comparison of dye degradation time using silver nanoparticles.

Sl No.	Nanoparticles	Dyes	Reaction Conditions	Removal (%)	Time	Ref.
1.	MMT/iron oxide/Ag	Rhodamine B	Catalyst: 0.448 mg/mL; NaBH4: 27 mM; Dye: 0.08 mM.	46.0	8 min	[30]
2.	Ag NPs	Methylene blue	Catalyst: 0.1 mg/mL; Dye: 10 mg/L.	84.0	64 h	[55]
3.	Ag NPs	Safranin	Catalyst: 0.12 mg/mL; Dye: 10 mg/L.	84.6	72 h	[56]
4.	Au-AgNPs	Malachite green	Catalyst: 0.1 mg/mL; Dye: 40 mg/L.	90.0	48 h	[57]
5.	Bentonite-Ag^0	Malachite green	Catalyst: 0.12 mg/mL; Dye: 5×10^{-5} M.	86.4	5 min	[58]
6.	AgNPs	crystal violet	Catalyst: 10 mg/mL; Dye: NA.	90.0	24 h	[59]
7.	AgNPs	Methylene blue	Catalyst: 0.3 mg/mL; Dye: 3.1×10^{-5} M. NaBH4: 3.0×10^{-5} M.	100	1 min	[60]
8.	Au-Ag NPs	Congo red	Catalyst: 20 µL; Dye: 10^{-4} M. NaBH4: 20 µL.	100	6 min	[32]
9.	Ag NPs	Methylene blue	Catalyst: 2 mL; Dye: 10^{-3} M. NaBH4: 0.1 M	100	13 min	[61]
10.	Fe_3O_4 @PDA-Ag	Methylene blue	Catalyst: 3 mg; Dye: 20 mg/L. NaBH4: 0.1 M	92.6	7 min	[62]
11.	AS-AgNPs	Methylene blue	Catalyst: 0.05 mL; Dye: 100 µM. NaBH4: 100 mM	97.0	27 min	[63]
12.	AgNPs	Methylene blue	Catalyst: 0.05 mL; Dye: 50 µM. NaBH4: 0.005 M	99.0	20 min	[64]
13.	Ag-iron oxide NPs	Crystal violet Malachite green Mixture (1:1 v/v)	Catalyst: 0.5 mL; Dye: 100 mg/L. NaBH4: 0.5 mg/mL	100	3 min	This work

4. Conclusions

Here, silver-iron oxide nanoparticles were synthesized using kulekhara leaves extract. The synthesis approach is simple, facile, low-cost, and eco-friendly. The synthesized nanoparticles were characterized by UV-Vis, FTIR, XRD, and STEM-Cs analysis. The findings proved the formation of Ag-Fe_2O_3 nanoparticles (10.42 ± 0.81 nm). The green nanoparticles were used to degrade azo bonds in crystal violet, malachite green, and their mixture in the presence of sodium borohydride. Results exhibited the rapid degradation of dye molecules (~100%) within three minutes. These findings could entice the researcher to design and develop the catalytic degradation of azo bonds of various dye molecules in wastewater.

Author Contributions: H.K.: Conceptualization, Formal analysis, Investigation, Writing: original draft, Writing: review and editing. C.-W.K.: Project administration, Funding acquisition, Writing: review and editing. All authors have read and agreed to the published version of the manuscript.

Funding: Basic Science Research Program supported this research through the National Research Foundation of Korea, funded by the Ministry of Education (NRF-2019R1I1A3A02059471) and was supported under the framework of an international cooperation program managed by the National Research Foundation of Korea (NRF-2020K2A9A2A08000181).

Institutional Review Board Statement: Not applicable.

Informed Consent Statement: Not applicable.

Data Availability Statement: Not applicable.

Conflicts of Interest: The authors declare that they have no known competing financial interest or personal relationships that could have appeared to influence the work reported in this paper. Moreover, no animal studies or human participants are involved in this study.

References

1. Oyelude, E.O.; Awudza, J.A.M.; Twumasi, S.K. Removal of malachite green from aqueous solution using pulverized teak leaf litter: Equilibrium, kinetic and thermodynamic studies. *Chem. Cent. J.* **2018**, *12*, 81. [CrossRef]
2. Martins, L.R.; Catone Soares, L.; Alves Gurgel, L.V.; Gil, L.F. Use of a new zwitterionic cellulose derivative for removal of crystal violet and orange II from aqueous solutions. *J. Hazard. Mater.* **2022**, *424*, 127401. [CrossRef]
3. Adegoke, K.A.; Bello, O.S. Dye sequestration using agricultural wastes as adsorbents. *Water Resour. Ind.* **2015**, *12*, 8–24. [CrossRef]
4. Ozlem-Caliskan, S.; Ilikci-Sagkan, R.; Karakas, H.; Sever, S.; Yildirim, C.; Balikci, M.; Ertabaklar, H. Efficacy of malachite green mediated photodynamic therapy on treatment of Cutaneous Leishmaniasis: In vitro study. *Photodiagnosis Photodyn. Ther.* **2022**, *40*, 103111. [CrossRef] [PubMed]
5. Castro, J.; Lima, Â.; Sousa, L.G.V.; Rosca, A.S.; Muzny, C.A.; Cerca, N. Crystal Violet Staining Alone Is Not Adequate to Assess Synergism or Antagonism in Multi-Species Biofilms of Bacteria Associated with Bacterial Vaginosis. *Front. Cell. Infect. Microbiol.* **2022**, *11*, 1375. [CrossRef]
6. Krishna Moorthy, A.; Govindarajan Rathi, B.; Shukla, S.P.; Kumar, K.; Shree Bharti, V. Acute toxicity of textile dye Methylene blue on growth and metabolism of selected freshwater microalgae. *Environ. Toxicol. Pharmacol.* **2021**, *82*, 103552. [CrossRef]
7. Oladoye, P.O.; Bamigboye, O.M.; Ogunbiyi, O.D.; Akano, M.T. Toxicity and decontamination strategies of Congo red dye. *Groundw. Sustain. Dev.* **2022**, 100844. [CrossRef]
8. Littlefield, N.A.; Blackwell, B.-N.; Hewitt, C.C.; Gaylor, D.W. Chronic Toxicity and Carcinogenicity Studies of Gentian Violet in Mice. *Toxicol. Sci.* **1985**, *5*, 902–912. [CrossRef]
9. Kolya, H.; Tripathy, T. Hydroxyethyl Starch-g-Poly-(N,N-dimethylacrylamide-co-acrylic acid): An efficient dye removing agent. *Eur. Polym. J.* **2013**, *49*, 4265–4275. [CrossRef]
10. Haque, A.N.; Sultana, N.; Sayem, A.S.; Smriti, S.A. Sustainable Adsorbents from Plant-Derived Agricultural Wastes for Anionic Dye Removal: A Review. *Sustainability* **2022**, *14*, 11098. [CrossRef]
11. Wang, X.; Zhang, P.; Xu, F.; Sun, B.; Hong, G.; Bao, L. Adsorption of Methylene Blue on Azo Dye Wastewater by Molybdenum Disulfide Nanomaterials. *Sustainability* **2022**, *14*, 7585. [CrossRef]
12. Alam, J.; Shukla, A.K.; Ansari, M.A.; Ali, F.A.; Alhoshan, M. Dye Separation and Antibacterial Activities of Polyaniline Thin Film-Coated Poly(phenyl sulfone) Membranes. *Membranes* **2021**, *11*, 25. [CrossRef] [PubMed]
13. Kolya, H.; Sasmal, D.; Tripathy, T. Novel Biodegradable Flocculating Agents Based on Grafted Starch Family for the Industrial Effluent Treatment. *J. Polym. Environ.* **2017**, *25*, 408–418. [CrossRef]
14. Pinheiro, L.R.; Gradíssimo, D.G.; Xavier, L.P.; Santos, A. V Degradation of Azo Dyes: Bacterial Potential for Bioremediation. *Sustainability* **2022**, *14*, 1510. [CrossRef]
15. Kolya, H.; Kuila, T.; Kim, N.H.; Lee, J.H. Bioinspired silver nanoparticles/reduced graphene oxide nanocomposites for catalytic reduction of 4-nitrophenol, organic dyes and act as energy storage electrode material. *Compos. Part B Eng.* **2019**, *173*, 106924. [CrossRef]
16. Kang, C.-W.; Kolya, H. Green Synthesis of Ag-Au Bimetallic Nanocomposites Using Waste Tea Leaves Extract for Degradation Congo Red and 4-Nitrophenol. *Sustainability* **2021**, *13*, 3318. [CrossRef]
17. You, X.; Zhou, R.; Zhu, Y.; Bu, D.; Cheng, D. Adsorption of dyes methyl violet and malachite green from aqueous solution on multi-step modified rice husk powder in single and binary systems: Characterization, adsorption behavior and physical interpretations. *J. Hazard. Mater.* **2022**, *430*, 128445. [CrossRef]
18. Cuong, D.V.; Hou, C.-H. Engineered biochar prepared using a self-template coupled with physicochemical activation for highly efficient adsorption of crystal violet. *J. Taiwan Inst. Chem. Eng.* **2022**, *139*, 104533. [CrossRef]

19. Kumar, S.A.; Jarvin, M.; Inbanathan, S.S.R.; Umar, A.; Lalla, N.P.; Dzade, N.Y.; Algadi, H.; Rahman, Q.I.; Baskoutas, S. Facile green synthesis of magnesium oxide nanoparticles using tea (Camellia sinensis) extract for efficient photocatalytic degradation of methylene blue dye. *Environ. Technol. Innov.* **2022**, *28*, 102746. [CrossRef]
20. Liu, Y.; Zheng, H.; Sun, Y.; Ren, J.; Zheng, X.; Sun, Q.; Jiang, S.; Ding, W. Synthesis of novel chitosan-based flocculants with amphiphilic structure and its application in sludge dewatering: Role of hydrophobic groups. *J. Clean. Prod.* **2020**, *249*, 119350. [CrossRef]
21. Ji, Y.; Ma, C.; Li, J.; Zhao, H.; Chen, Q.; Li, M.; Liu, H. A Magnetic Adsorbent for the Removal of Cationic Dyes from Wastewater. *Nanomaterials* **2018**, *8*, 710. [CrossRef]
22. Liu, X.; Tian, J.; Li, Y.; Sun, N.; Mi, S.; Xie, Y.; Chen, Z. Enhanced dyes adsorption from wastewater via Fe3O4 nanoparticles functionalized activated carbon. *J. Hazard. Mater.* **2019**, *373*, 397–407. [CrossRef]
23. Gallo-Cordova, A.; Castro, J.J.; Winkler, E.L.; Lima, E.; Zysler, R.D.; del Puerto Morales, M.; Ovejero, J.G.; Streitwieser, D.A. Improving degradation of real wastewaters with self-heating magnetic nanocatalysts. *J. Clean. Prod.* **2021**, *308*, 127385. [CrossRef]
24. Kolya, H.; Mondal, S.; Kang, C.W.; Nah, C. The use of polymer-graphene composites in catalysis. In *Polymer Nanocomposites Containing Graphene*; Woodhead Publishing: Sawston, UK, 2022; pp. 537–556. [CrossRef]
25. Kouhbanani, M.A.J.; Beheshtkhoo, N.; Taghizadeh, S.; Amani, A.M.; Alimardani, V. One-step green synthesis and characterization of iron oxide nanoparticles using aqueous leaf extract of *Teucrium polium* and their catalytic application in dye degradation. *Adv. Nat. Sci. Nanosci. Nanotechnol.* **2019**, *10*, 15007. [CrossRef]
26. Barozzi, M.; Copelli, S.; Russo, E.; Sgarbossa, P.; Lavagnolo, M.C.; Sandon, A.; Morosini, C.; Sieni, E. Implementation of Magnetic Nanostructured Adsorbents for Heavy Metals Separation from Textile Wastewater. *Sustainability* **2022**, *14*, 11785. [CrossRef]
27. Biswas, S.; Pal, A. Application of biopolymers as a new age sustainable material for surfactant adsorption: A brief review. *Carbohydr. Polym. Technol. Appl.* **2021**, *2*, 100145. [CrossRef]
28. Qi, Y.; Yang, M.; Xu, W.; He, S.; Men, Y. Natural polysaccharides-modified graphene oxide for adsorption of organic dyes from aqueous solutions. *J. Colloid Interface Sci.* **2017**, *486*, 84–96. [CrossRef] [PubMed]
29. Pandey, N.; Shukla, S.K.; Singh, N.B. Water purification by polymer nanocomposites: An overview. *Nanocomposites* **2017**, *3*, 47–66. [CrossRef]
30. Acar, M.K.; Altun, T.; Gubbuk, I.H. Synthesis and characterization of silver doped magnetic clay nanocomposite for environmental applications through effective RhB degradation. *Int. J. Environ. Sci. Technol.* **2022**. [CrossRef]
31. Sengan, M.; Veeramuthu, D.; Veerappan, A. Photosynthesis of silver nanoparticles using Durio zibethinus aqueous extract and its application in catalytic reduction of nitroaromatics, degradation of hazardous dyes and selective colorimetric sensing of mercury ions. *Mater. Res. Bull.* **2018**, *100*, 386–393. [CrossRef]
32. Pandey, S.; Do, J.Y.; Kim, J.; Kang, M. Fast and highly efficient catalytic degradation of dyes using κ-carrageenan stabilized silver nanoparticles nanocatalyst. *Carbohydr. Polym.* **2020**, *230*, 115597. [CrossRef]
33. Liu, X.; Xu, J.; Jing, K.; Lu, L.; Liu, H. Facile synthesis of Ag/AgCl/3D-rGO with rapid catalytic degradation toward Methyl Orange and Rhodamine B. *Chem. Eng. Res. Des.* **2022**, *186*, 22–33. [CrossRef]
34. Naseem, K.; Ali, F.; Tahir, M.H.; Afaq, M.; Yasir, H.M.; Ahmed, K.; muteb Aljuwayid, A.; Habila, M.A. Investigation of catalytic potential of sodium dodecyl sulfate stabilized silver nanoparticles for the degradation of methyl orange dye. *J. Mol. Struct.* **2022**, *1262*, 132996. [CrossRef]
35. Padre, S.M.; Kiruthika, S.; Mundinamani, S.; Ravikirana; Surabhi, S.; Jeong, J.-R.; Eshwarappa, K.M.; Murari, M.S.; Shetty, V.; Ballal, M.; et al. Mono- and Bimetallic Nanoparticles for Catalytic Degradation of Hazardous Organic Dyes and Antibacterial Applications. *ACS Omega* **2022**, *7*, 35023–35034. [CrossRef]
36. Baig, N.; Kammakakam, I.; Falath, W. Nanomaterials: A review of synthesis methods, properties, recent progress, and challenges. *Mater. Adv.* **2021**, *2*, 1821–1871. [CrossRef]
37. Chakravarty, A.; Ahmad, I.; Singh, P.; Ud Din Sheikh, M.; Aalam, G.; Sagadevan, S.; Ikram, S. Green synthesis of silver nanoparticles using fruits extracts of Syzygium cumini and their bioactivity. *Chem. Phys. Lett.* **2022**, *795*, 139493. [CrossRef]
38. Kolya, H.; Maiti, P.; Pandey, A.; Tripathy, T. Green synthesis of silver nanoparticles with antimicrobial and azo dye (Congo red) degradation properties using Amaranthus gangeticus Linn leaf extract. *J. Anal. Sci. Technol.* **2015**, *6*, 33. [CrossRef]
39. Basalius, H.; Mani, A.; Michael, A.; Mary, S.M.; Lenin, M.; Chelliah, P.; Siddiqui, M.R.; Wabaidur, S.M.; Islam, M.A. Green synthesis of nano-silver using Syzygium samarangense flower extract for multifaceted applications in biomedical and photocatalytic degradation of methylene blue. *Appl. Nanosci.* **2022**. [CrossRef]
40. Panyala, N.R.; Peña-Méndez, E.M.; Havel, J. Silver or silver nanoparticles: A hazardous threat to the environment and human health? *J. Appl. Biomed.* **2008**, *6*, 117–129. [CrossRef]
41. Roy, M.; Sarkar, B.C.; Shukla, G.; Vineeta; Debnath, M.K.; Nath, A.J.; Bhat, J.A.; Chakravarty, S. Traditional homegardens and ethnomedicinal plants: Insights from the Indian Sub-Himalayan region. *Trees For. People* **2022**, *8*, 100236. [CrossRef]
42. Konar, A.; Mukherjee, K.; Ghosh, P.; El-Shazly, M. Traditional medicinal plants used in different districts of West Bengal by the tribal communities. *J. Pharmacogn. Phytochem.* **2022**, *11*, 104–110. [CrossRef]
43. Sethiya, N.K.; Ahmed, N.M.; Shekh, R.M.; Kumar, V.; Kumar Singh, P.; Kumar, V. Ethnomedicinal, phytochemical and pharmacological updates on Hygrophila auriculata (Schum.) Hiene: An overview. *J. Integr. Med.* **2018**, *16*, 299–311. [CrossRef] [PubMed]

44. Mubeen, B.; Rasool, M.G.; Ullah, I.; Rasool, R.; Imam, S.S.; Alshehri, S.; Ghoneim, M.M.; Alzarea, S.I.; Nadeem, M.S.; Kazmi, I. Phytochemicals Mediated Synthesis of AuNPs from Citrullus colocynthis and Their Characterization. *Molecules* **2022**, *27*, 1300. [CrossRef]
45. Yin, Y.; Han, D.; Tai, C.; Tan, Z.; Zhou, X.; Yu, S.; Liu, J.; Jiang, G. Catalytic role of iron in the formation of silver nanoparticles in photo-irradiated Ag+-dissolved organic matter solution. *Environ. Pollut.* **2017**, *225*, 66–73. [CrossRef]
46. Khalil, A.T.; Ovais, M.; Ullah, I.; Ali, M.; Shinwari, Z.K.; Maaza, M. Biosynthesis of iron oxide (Fe2O3) nanoparticles via aqueous extracts of Sageretia thea (Osbeck.) and their pharmacognostic properties. *Green Chem. Lett. Rev.* **2017**, *10*, 186–201. [CrossRef]
47. Masek, A.; Latos-Brozio, M.; Chrzescijanska, E.; Podsedek, A. Polyphenolic Profile and Antioxidant Activity of *Juglans regia* L. Leaves and Husk Extracts. *Forests* **2019**, *10*, 988. [CrossRef]
48. Kolya, H.; Kuila, T.; Kim, N.H.; Lee, J.H. Colorimetric/naked eye detection of arsenic ions in aqueous medium by mango flower extract: A facile and novel approach. *Appl. Surf. Sci.* **2020**, *513*, 145760. [CrossRef]
49. Nalbandian, L.; Patrikiadou, E.; Zaspalis, V.; Patrikidou, A.; Hatzidaki, E.; N. Papandreou, C. Magnetic nanoparticles in medical diagnostic applications: Synthesis, characterization and proteins conjugation. *Curr. Nanosci.* **2016**, *12*, 455–468. [CrossRef]
50. Raj, S.; Chand Mali, S.; Trivedi, R. Green synthesis and characterization of silver nanoparticles using Enicostemma axillare (Lam.) leaf extract. *Biochem. Biophys. Res. Commun.* **2018**, *503*, 2814–2819. [CrossRef]
51. Joya, M.R.; Barón-Jaimez, J.; Barba-Ortega, J. Preparation and characterization of Fe_2O_3nanoparticles. *J. Phys. Conf. Ser.* **2013**, *466*, 12004. [CrossRef]
52. Jang, M.-S.; Lee, Y.-M.; Kim, C.-H.; Lee, J.-H.; Kang, D.-W.; Kim, S.-J.; Lee, Y.-C. Triphenylmethane reductase from *Citrobacter* sp. strain KCTC 18061P: Purification, characterization, gene cloning, and overexpression of a functional protein in *Escherichia coli*. *Appl. Environ. Microbiol.* **2005**, *71*, 7955–7960. [CrossRef]
53. Henderson, A.L.; Schmitt, T.C.; Heinze, T.M.; Cerniglia, C.E. Reduction of malachite green to leucomalachite green by intestinal bacteria. *Appl. Environ. Microbiol.* **1997**, *63*, 4099–4101. [CrossRef]
54. Sreekanth, T.V.M.; Nagajyothi, P.C.; Reddy, G.R.; Shim, J.; Yoo, K. Urea assisted ceria nanocubes for efficient removal of malachite green organic dye from aqueous system. *Sci. Rep.* **2019**, *9*, 14477. [CrossRef] [PubMed]
55. Shukla, S.; Kashyap, A.; Kashyap, A.; Vishwakarma, D.; Maholiya, A. Methylene Blue Dye Degradation Using Silver Nanoparticles Synthesized from Andographis Paniculata Leaves Extract. *J. Pharm. Res. Int.* **2021**, *33*, 131–139.
56. Abd El-Aziz, A.R.M.; Gurusamy, A.; Alothman, M.R.; Shehata, S.M.; Hisham, S.M.; Alobathani, A.A. Silver nanoparticles biosynthesis using Saussurea costus root aqueous extract and catalytic degradation efficacy of safranin dye. *Saudi J. Biol. Sci.* **2021**, *28*, 1093–1099. [CrossRef]
57. Ojo, S.A.; Lateef, A.; Azeez, M.A.; Oladejo, S.M.; Akinwale, A.S.; Asafa, T.B.; Yekeen, T.A.; Akinboro, A.; Oladipo, I.C.; Gueguim-Kana, E.B.; et al. Biomedical and Catalytic Applications of Gold and Silver-Gold Alloy Nanoparticles Biosynthesized Using Cell-Free Extract of Bacillus Safensis LAU 13: Antifungal, Dye Degradation, Anti-Coagulant and Thrombolytic Activities. *IEEE Trans. Nanobiosci.* **2016**, *15*, 433–442. [CrossRef] [PubMed]
58. Diana-Carmen, M.; Dumitra, R.; Ana-Maria, G.; Ana-Maria, R.; Andrei, C.V.; Valentin, Z.; Ileana-Denisa, N. Silver Nanoparticles Incorporated on Natural Clay as an Inhibitor against the New ISO SS Bacteria Isolated from Sewage Sludge, Involved in Malachite Green Dye Oxidation. *Molecules* **2022**, *27*, 5791. [CrossRef] [PubMed]
59. Nga, N.T.A.; Raghavendra, V.B.; Sindhu, R.; Alshiekheid, M.; Sabour, A.; Krishnan, R.; Lan Chi, N.T.; Pugazhendhi, A. Green fabrication of silver nanoparticles using Chloroxylon swietenia leaves and their application towards dye degradation and food borne pathogens. *Food Chem. Toxicol.* **2022**, *165*, 113192. [CrossRef]
60. Recio-Sánchez, G.; Tighe-Neira, R.; Alvarado, C.; Inostroza-Blancheteau, C.; Benito, N.; García-Rodríguez, A.; Marcos, R.; Pesenti, H.; Carmona, E.R. Assessing the effectiveness of green synthetized silver nanoparticles with Cryptocarya alba extracts for remotion of the organic pollutant methylene blue dye. *Environ. Sci. Pollut. Res.* **2019**, *26*, 15115–15123. [CrossRef] [PubMed]
61. Bonnia, N.N.; Kamaruddin, M.S.; Nawawi, M.H.; Ratim, S.; Azlina, H.N.; Ali, E.S. Green Biosynthesis of Silver Nanoparticles Using 'Polygonum Hydropiper' and Study its Catalytic Degradation of Methylene Blue. *Procedia Chem.* **2016**, *19*, 594–602. [CrossRef]
62. Zhang, N.; Peng, S.; Liu, Z.; Li, Y.; Huang, J.; Li, J.; Wan, H.; Zhou, S.; Gao, Z.; Chen, T. Ag NPs decorated on the magnetic Fe3O4@PDA as efficient catalyst for organic pollutants removal and as effective antimicrobial agent for microbial inhibition. *J. Alloys Compd.* **2022**, *928*, 167257. [CrossRef]
63. Rajasekar, R.; Samuel, M.; Edison, T.N.J.I.; Raman, N. Sustainable synthesis of silver nanoparticles using Alstonia scholaris for enhanced catalytic degradation of methylene blue. *J. Mol. Struct.* **2021**, *1246*, 131208. [CrossRef]
64. Somasundaram, C.K.; Atchudan, R.; Edison, T.N.; Perumal, S.; Vinodh, R.; Sundramoorthy, A.K.; Babu, R.S.; Alagan, M.; Lee, Y.R. Sustainable Synthesis of Silver Nanoparticles Using Marine Algae for Catalytic Degradation of Methylene Blue. *Catalysts* **2021**, *11*, 1377. [CrossRef]